Chemical Engineering Journal 225 (2013) 766–775

Contents lists available at SciVerse ScienceDirect

Chemical Engineering Journal

journal homepage: www.elsevier.com/locate/cej

Synthesis of PPy-modified TiO_2 composite in H_2SO_4 solution and its novel adsorption characteristics for organic dyes

Jingjing Li [a], Qian Zhang [a], Jiangtao Feng [a,*], Wei Yan [b,*]

[a] Department of Environmental Science and Engineering, Xi'an Jiaotong University, Xi'an 710049, PR China
[b] State Key Laboratory of Multiphase Flow in Power Engineering, Xi'an Jiaotong University, Xi'an 710049, PR China

HIGHLIGHTS

- The novel PPy/TiO_2 composite has a potential to treat dye wastewater.
- The H_2SO_4 concentration affects the adsorption ability of the composites.
- The selective adsorption by PPy/TiO_2 can be complete by changing its surface charge.
- The equilibrium adsorption is achieved in a short time of 30 min.
- The composite adsorbent can be reused repeatedly with a high adsorption capacity.

GRAPHICAL ABSTRACT

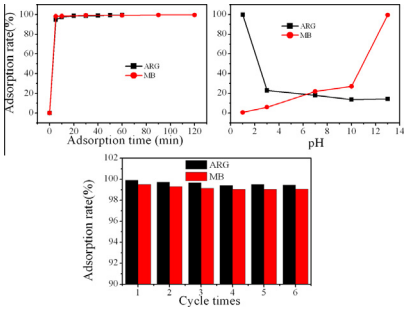

ARTICLE INFO

Article history:
Received 5 December 2012
Received in revised form 1 March 2013
Accepted 5 March 2013
Available online 14 March 2013

Keywords:
TiO_2
Polypyrrole
Composite adsorbent
H_2SO_4
Dye adsorption
Regeneration

ABSTRACT

The PPy/TiO_2 and PPy/P25 composites prepared via the in situ polymerization in H_2SO_4 solution with different concentrations were studied for Acid Red G (ARG) or Methylene Blue (MB) adsorption. Their physicochemical properties were examined by X-ray diffraction (XRD), Fourier transform infrared spectroscopy (FT-IR), thermogravimetric analysis (TGA) and zeta potential analysis. The results showed that the H_2SO_4 concentration and the property of metal oxide (self-prepared TiO_2 or commercial P25) obviously affected the nature and adsorption abilities of the PPy/TiO_2 and PPy/P25 composites. The composites can adsorb Acid Red G (ARG) or Methylene Blue (MB) rapidly and reach the equilibrium in 30 min. The adsorption amount of ARG on the composites decreased with the increase of pH value, while the MB removal efficiency increased with pH increase. The adsorption behaviors of ARG and MB on the composites were described by the pseudo-second-order and Langmuir isotherm models. According to the Langmuir isotherm, the PPy/TiO_2 composites exhibited larger maximum adsorption amount than PPy/P25, especially with the PPy/TiO_2 composite prepared in 0.16 mol/L H_2SO_4 (0.16 M-PPy/TiO_2), on which the maximum adsorption amounts of ARG and MB were 218.82 and 323.62 mg/g, respectively. Regeneration experiments revealed that the 0.16 M-PPy/TiO_2 composite can be regenerated easily and reused for six times without visible loss of its original capacity. Additionally, its adsorption efficiencies of ARG and MB in real effluents were still higher than 87% after adsorption–desorption for four times. Through comparing the FT-IR spectra of PPy/TiO_2 before and after adsorption, as well as the surface charge measurement, it can be speculated that electrostatic interaction, hydrogen bonding and specific chemical interaction may be the possible mechanism for the adsorption of ARG and MB by the PPy/TiO_2 composites.

* Corresponding authors.
E-mail addresses: fjtes@mail.xjtu.edu.cn (J. Feng), yanwei@mail.xjtu.edu.cn (W. Yan).

1385-8947/$ - see front matter © 2013 Elsevier B.V. All rights reserved.
http://dx.doi.org/10.1016/j.cej.2013.03.011

1. Introduction

Recently, many studies have focused on using TiO_2 as adsorbent, mainly because of its low cost, simple preparation, good stability and non-toxic nature [1–4]. Besides, the hydroxyl groups which present on the surface of TiO_2 can interact with the pollutant molecules, thereby realizing the adsorption of the pollutants [2]. However, the adsorption capacity of TiO_2 was not high compared with that of activated carbon [5–8]. What is more, the studies on the regeneration of TiO_2 are extremely rare, probably due to its low regeneration efficiency [2]. Therefore, the improvement in the adsorption and regeneration capacities of TiO_2 through modification with other materials is highly desired. Some publications have reported that the modified TiO_2 showed better adsorption capacity than the pristine TiO_2 [1,4]. Janus et al. [1] compared the adsorption capacities of unmodified and carbon modified TiO_2, and found the adsorption ability of TiO_2 was improved at least 10 times by modification.

Polypyrrole (PPy) has been used as a modifier for TiO_2 in many studies because of its high thermal stability and non-toxicity [9]. In fact, it is recognized that PPy also has the adsorption ability through ion exchange or electrostatic interaction, largely owing to the existence of positively charged nitrogen atoms in PPy matrix [10–13]. Moreover, PPy can undergo protonation or deprotonation processes when it is immersed in acid or alkali solution, respectively, which results in the change of its surface charges, followed by doping or dedoping of counter ions [14,15]. The capability of reversible transformation of PPy makes it possible that the ions could be adsorbed on or desorbed from PPy, hence, we speculate that it would have an excellent adsorption–desorption property. In this regard, PPy can be considered as a potential modifier to improve the adsorption and regeneration capacities of TiO_2.

Besides, the nature of the prepared TiO_2 and PPy would be affected by the solution pH, and then their adsorption performance would be impacted as well. Dunphy-Guzman et al. [16] investigated the aggregation behavior of TiO_2 particles with different polymorphs as the function of pH, and indicated that the pH value affected the surface adsorption and reactivity of TiO_2 particles. In addition, the crystal structure of TiO_2 was also affected by pH. Tang et al. [17] pointed out that the crystal form of TiO_2 was changed from amorphous to anatase, and then to rutile with the decrease of pH value. Some publications have reported that the adsorption capacity of adsorbent would change with its crystal form [18,19]. On the other hand, PPy can undergo molecular structure or composition changes at the solid/solution interface under different solution pH conditions, making PPy display various surface electric properties, followed by affecting its adsorption performance [15]. In this work, we synthesized a series of PPy-modified TiO_2 (PPy/TiO_2) composite adsorbents in H_2SO_4 solution with various concentrations. Their physicochemical properties were characterized. Also, their adsorption and regeneration properties for Acid Red G (ARG) and Methylene Blue (MB) were studied. The results indicated that the adsorption properties of the composites were affected by H_2SO_4 concentration. Moreover, the composites have different adsorption capacities for anionic and cationic dyes by preprocessing them in solutions with different pH values. This suggested that the PPy/TiO_2 composites may have a potential in selectively adsorbing dyes.

2. Experimental

2.1. Materials

Pyrrole (98%, Qingquan Pharmaceutical & Chemical Ltd., Zhejiang, China) was distilled twice under reduced pressure, and then refrigerated and stored in the dark under nitrogen. P25 power (Evonik Degussa) was obtained from Guangzhou HuaLiSen Trade Co., China. Acid Red G (ARG, 509.43 g/mol) was commercial grade and purified before used. Methylene Blue (MB, 319.86 g/mol) was purchased from Beijing Chemical Reagent Co., China. The structures are shown in Fig. S1. $FeCl_3{\cdot}6H_2O$, HNO_3 (65–68%), H_2SO_4 (98%), CH_3COOH, NaOH, Na_2SO_4, n-propanol (99.9%), sodium dodecyl benzene sulfonate (SDBS), cetyl trimethyl ammonium bromide (CTAB), anhydrous ethanol and tetrabutyl titanate (TBOT, 98%) were of analytical reagent grades and used without further purification. The real effluent used in our study was derived from the printing and dyeing factory in Xi'an. The deionized water used for all the experiments was obtained by an EPED-40TF Superpure Water System (EPED, China).

2.2. Synthesis of adsorbents

The PPy/TiO_2 composites were synthesized by the chemical oxidative polymerization of pyrrole monomer in the pre-prepared TiO_2 suspension solutions with different H_2SO_4 concentrations. The detailed process was described as follows. First, a mixture of TBOT and n-propanol (the volume ratio is 5:2) was added into 200 mL H_2SO_4 solution with different concentrations (0.08, 0.16 and 0.24 mol/L), with magnetic stirring for 24 h. Then the formed suspension solution was cooled to 5 °C, followed by adding 0.675 mL of pyrrole monomer with stirring for 30 min. 25 mL $FeCl_3$ (1.0 mol/L) solution was added dropwise to this mixture, and then the mixed solution was stirred for another 24 h. Finally, the PPy/TiO_2 composites were filtrated and washed with deionized water. The prepared composites, named as 0.08 M-PPy/TiO_2, 0.16 M-PPy/TiO_2 and 0.24 M-PPy/TiO_2 according to the concentration of H_2SO_4, were dried at 50 °C for 24 h.

For comparison, the PPy/P25 composite was also synthesized with the same procedure, except that P25 (2.34 g) was employed instead of self-prepared TiO_2.

2.3. Characterization

X-ray diffraction pattern was obtained with an X'Pert PRO MRD Diffractometer using Cu Kα radiation. Fourier transform infrared spectra (FT-IR) of samples were measured by the KBr pellet method on a BRUKER TENSOR 37 FT-IR spectrophotometer in the range of 4000–400 cm^{-1}. The thermogravimetric (TG) analyses were performed on Setaram Labsys Evo in N_2 flow and at a heating rate of 10 °C/min. The sample morphology was characterized by scanning electron microscopy (SEM, JSM-6700F, Japan). Zeta potentials of samples were measured with Malvern Zetasizer Nano ZS90. It was prepared by adding 5 mg of sample in a 10 mL NaCl solution (10^{-3} mol/L) at different pH values (adjusted with diluted HNO_3 or NaOH solution). The BET surface area (S_{BET}), total pore volume (V) and average pore radius (R) were measured at 77 K using Builder SSA-4200 (Beijing, China).

2.4. Adsorption experiments

All adsorption experiments were carried out in the dark condition at ambient temperature. The suspension containing 300 mg/L of ARG or MB solution and 2 g/L of adsorbent was stirred for 60–120 min. Then the suspension was centrifuged at 4000 rpm for 5 min. The supernatant was analyzed by the UV–Vis spectrophotometer (Agilent 8453). The absorbance values of MB and ARG were read at the wavelength of 665 and 503 nm, respectively.

In order to study the influence of the adsorbent surface potential on the adsorption capacities, the adsorbents were pretreated by HNO_3 or NaOH solutions (pH = 1.0–13.0). Then the treated adsorbents were used to adsorb the same concentration of ARG or MB

solution. The effect of ionic concentration (0–0.3 mol/L) on the adsorption was carried out by adding Na_2SO_4 into the 300 mg/L ARG or MB solution. The influence of surfactant on the adsorption was performed by adding SDBS (0–4.0 CMC) into 300 mg/L ARG solution or adding CTAB (0–4.0 CMC) into 300 mg/L MB solution.

The adsorption rate R (%) and the amount of dye molecules adsorbed onto the adsorbents Q_t (mg/g) in a certain time t were calculated from the following equations respectively:

$$R = \frac{C_0 - C_t}{C_0} \times 100 \quad (1)$$

$$Q_t = \frac{C_0 - C_t}{M} \times V \quad (2)$$

where C_0 is the initial concentration (mg/L); C_t is the residual concentration at time t (mg/L); V is the solution volume (L), and M is the adsorbent mass (g).

The adsorption equilibrium of ARG or MB (300 mg/L) was evaluated at 25 °C. The adsorption kinetics was investigated using the pseudo-first-order and pseudo-second-order models, according to the following equations respectively:

$$\lg(Q_{eq} - Q_t) = \lg Q_{eq} - \frac{K_1}{2.303} t \quad (3)$$

$$\frac{t}{Q_t} = \frac{1}{K_2 Q_{eq}^2} + \frac{t}{Q_{eq}} \quad (4)$$

where t is the adsorption time (min); K_1 (1/min) and K_2 (g/mg/min$^{0.5}$) are the rate constants for the pseudo-first-order and pseudo-second-order models, respectively; Q_{eq} (mg/g) is adsorption amount at equilibrium state.

For comparison, ARG and MB effluents (300 mg/L) were prepared by dissolving ARG and MB powder into the real effluent instead of deionized water. The adsorption experiments of ARG and MB effluents were the same as that of ARG and MB solutions, and their concentrations were determined with UV–Vis spectrophotometer.

2.5. Adsorption isotherms

Adsorption isotherms of MB and ARG at 298 K were obtained by mixing different concentrations (100–800 mg/L) of MB or ARG solutions with 2 g/L of adsorbent, respectively. There are two models, Langmuir isotherm and Freundlich isotherm, which are described in linear forms according to the following equations respectively:

$$\frac{C_t}{Q_t} = \frac{1}{Q_{max} K_L} + \frac{C_t}{Q_{max}} \quad (5)$$

$$\log Q_t = \log K_F + n \log C_t \quad (6)$$

where Q_{max} (mg/g) is the maximum adsorption capacity; K_L (L/mg) is a constant related to the heat of adsorption; K_F (mg/g (mg/L)$^{-n}$) represents the adsorption capacity when C_t equals 1 and n represents the degree of dependence of adsorption on equilibrium concentration.

For thermomechanical analysis, the adsorption isotherm experiments were repeated at 288 and 308 K.

2.6. Regeneration experiments

In order to evaluate the regeneration ability of the composite adsorbent, the desorption processes of MB or ARG adsorbed on PPy/TiO_2 were studied by using ethanol, acid and alkali separately for treatment for 60 min. After centrifugation, the dye concentration was measured to calculate the desorption efficiency. Then the desorbed PPy/TiO_2 was activated with NaOH (0.1 mol/L) solution for the further adsorption of MB, and HNO_3 (0.1 mol/L) solution for ARG. The desorption efficiency (DE,%) was calculated by the following equation:

$$DE = \frac{C_a - C_d}{C_a} \quad (7)$$

where C_a is the adsorbed dye concentration and C_d is the desorbed dye concentration.

3. Results and discussion

3.1. Characterization of the samples

3.1.1. Characterization analyses

Fig. 1 shows the XRD patterns of 0.08 M-PPy/TiO_2, 0.16 M-PPy/TiO_2, 0.24 M-PPy/TiO_2 and PPy/P25. The XRD results show that 0.08 M-PPy/TiO_2 was purely anatase, for the diffraction peaks at 25.3°, 37.8° and 48.1° correspond well to the (101), (004) and (200) planes of anatase TiO_2, respectively. Except the anatase structure, 0.16 M-PPy/TiO_2 and 0.24 M-PPy/TiO_2 also contain rutile structure, for the diffraction peaks at 27.5° and 41.2° belong to the (110) and (111) planes of rutile TiO_2, respectively. Besides, the rutile peak intensity rises with the increased H_2SO_4 concentration. This indicated that the crystal form of the composites was affected by the pH of solution and easily exhibited rutile structure in lower pH environment [17]. PPy/P25 is also a mixture of anatase and rutile. From the peak intensities of the four composites, it was

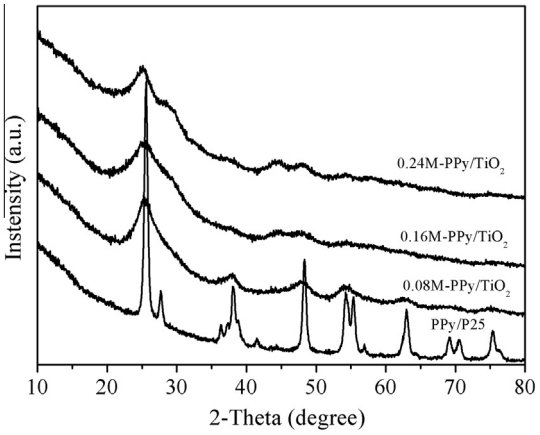

Fig. 1. XRD patterns of the PPy/TiO_2 and PPy/P25 composites.

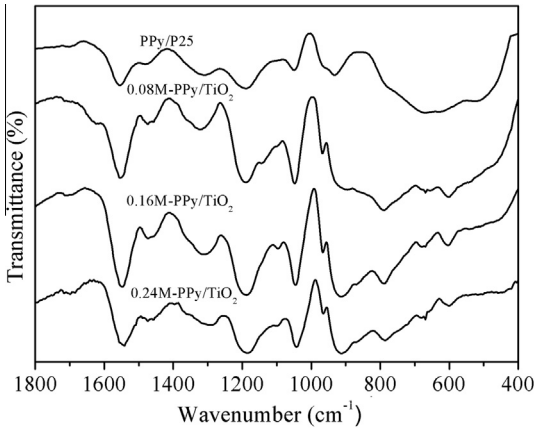

Fig. 2. FT-IR spectra of the PPy/TiO_2 and PPy/P25 composites.

Table 1
The FT-IR absorptions and their assignments.

Frequencies (cm^{-1})				Assignments
0.08 M-PPy/TiO_2	0.16 M-PPy/TiO_2	0.24 M-PPy/TiO_2	PPy/P25	
1552	1548	1543	1554	C–C stretching vibration [21,22]
1473	1471	1473	1481	C–N stretching vibration [21,22]
1321	1311	1294	1310	C–H or C–N in-plane deformation mode [21]
1190	1188	1186	1190	Sulfate anion [21]
1047	1045	1043	1049	C–H or N–H in-plane deformation vibration [21]
968	966	964	968	C–C out-of-plane deformation vibration [21]
914	914	912	933	C–H out-of-plane deformation vibration [21]
400–700				O–Ti–O [23]

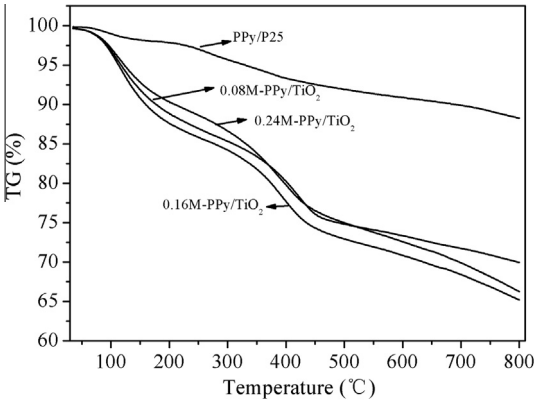

Fig. 3. TG analyses of the PPy/TiO_2 and PPy/P25 composites.

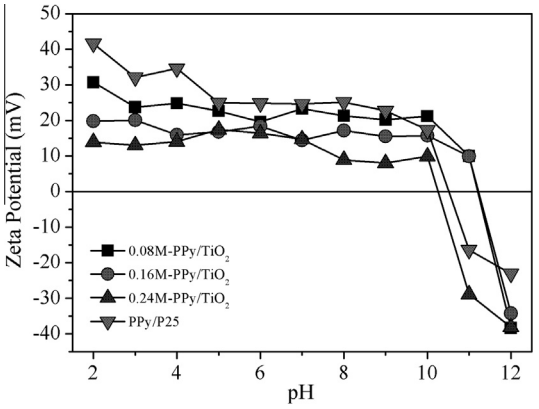

Fig. 4. Zeta potentials of the PPy/TiO_2 and PPy/P25 composites.

informed that the degree of crystallinity of PPy/TiO_2 composites was relatively low and mainly amorphous. It is also noted that no new peaks appear in the patterns of the three composites, suggesting that PPy was amorphous in the composite [20].

The FT-IR spectra (Fig. 2) and their assignments are listed in Table 1. The results demonstrated that the composites were formed. The intensities and positions of the bands related to PPy have many changes for the four composites, which may be owing to the various H_2SO_4 concentration and the property of the used metal oxide (self-prepared TiO_2 or commercial P25). This indicated that the four composites possessed different polymerization degrees and doping levels. This further resulted in the obvious variation of the intensities of the bands corresponded to O–Ti–O bending, which can be certified by the TG analyses (Fig. 3). Besides, the bands around 1188 cm^{-1} assigned to the sulfate anion are found in the spectra of the four composites, demonstrating that the sulfate anion entered PPy matrix was as doping ions [21]. The change of the peak intensity also suggested that the four composites were provided with different doping level.

Fig. 3 shows the TG analyses of 0.08 M-PPy/TiO_2, 0.16 M-PPy/TiO_2, 0.24 M-PPy/TiO_2 and PPy/P25. The first steep has about 8, 10, 7 and 1.5 wt.% below 150 °C for 0.08 M-PPy/TiO_2, 0.16 M-PPy/TiO_2, 0.24 M-PPy/TiO_2 and PPy/P25, respectively, which is attributed to the loss of the adsorbed water [24]. The second steep between 150 °C and 450 °C is probably assigned to the decomposition of PPy [25]. Based on the TG analyses, the amount of PPy in 0.08 M-PPy/TiO_2, 0.16 M-PPy/TiO_2, 0.24 M-PPy/TiO_2 and PPy/P25 were approximately calculated to be about 16, 17, 16 and 5.5 wt.%, respectively. This indicated that the PPy/TiO_2 composites contained more PPy than PPy/P25 did. PPy provided the adsorption sites, so it would have an enhanced adsorption capacity if the PPy content was increased. Therefore, the adsorption capacity of the PPy/TiO_2 composites would be higher than that of PPy/P25. The final weight lose (>450 °C) is possibly ascribed to the decomposition of the organics from the hydrolysis of TBOT and the sulfated anions chemically adsorbed on the surface of self-prepared TiO_2 and P25.

The textural properties of the PPy/TiO_2 and PPy/P25 composites are listed in Table 2. As observed, the S_{BET}, total pore volume and average pore radius of the PPy/TiO_2 composites vary with the

Table 2
The textural properties of the PPy/TiO_2 and PPy/P25 composites.

Samples	S_{BET} (m^2/g)	V (cm^3/g)	R (nm)
0.08 M-PPy/TiO_2	110.45	0.099	1.42
0.16 M-PPy/TiO_2	104.88	0.15	3.38
0.24 M-PPy/TiO_2	95.71	0.065	1.37
PPy/P25	47.02	0.34	14.45

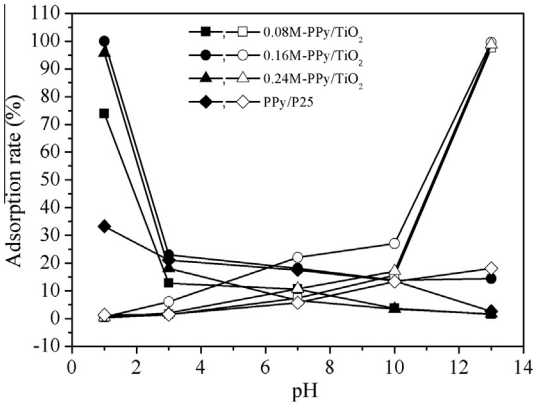

Fig. 5. Adsorption capacities of ARG (solid) and MB (hollow) on the PPy/TiO_2 and PPy/P25 composites pretreated with different pH solutions.

H_2SO_4 concentration. These changes are not very obvious. However, compared with the PPy/TiO_2 composites, PPy/P25 exhibited significant changes in the textural properties. This indicated that the effect for the properties of metal oxide on the textural properties of the composites was larger than that for the concentration of H_2SO_4. The PPy/TiO_2 composites have the enhanced S_{BET}, which is benefit for ARG and MB adsorption. While their reduced total pore volume and average pore radius may weaken their adsorption capacities for ARG and MB.

Fig. 4 shows the zeta potential values of 0.08 M-PPy/TiO_2, 0.16 M-PPy/TiO_2, 0.24 M-PPy/TiO_2 and PPy/P25 as a function of the solution pH. From Fig. 4, the zeta potentials of all samples are positive and do not have large changes in the pH range of 5–10. Additionally, the composites possessed different isoelectric point (pH_{iep}) owing to the H_2SO_4 concentration and the property of metal oxide. The isoelectric points of 0.08 M-PPy/TiO_2, 0.16 M-PPy/TiO_2, 0.24 M-PPy/TiO_2 and PPy/P25 are about 11.21, 11.23, 10.25 and 10.52, respectively.

3.2. Adsorption experiments

3.2.1. Effect of surface potential on the adsorption capacity

The adsorption capacities of these composites were altered when they were pretreated with acid or alkali solution, as shown in Fig. 5. The adsorption capacities of ARG on these composites increased with the decreasing pH and reached the largest adsorption amount at the pH of 1, proving that ARG could be easily adsorbed onto the acid-treated adsorbents. On the contrary, the adsorption capacities of MB enhanced with the increasing pH and reached the largest adsorption amount at the pH of 13, suggesting that MB could be easily adsorbed onto the alkali-treated adsorbents.

Zhang and Bai [15] pointed out that the surface of PPy could be positively charged or negatively charged in a solution with an appropriate range of pH according to the following equations:

$$PPyX + H^+ \leftrightarrow PPyXH^+, \quad pH < pH_{iep} \tag{8}$$

$$PPyX + OH^- \leftrightarrow PPyXOH^-, \quad pH > pH_{iep} \tag{9}$$

where X is the counter anion. According to the results of zeta potential analyses, the surface of the adsorbents was positively charged when the pH was below 10, while their surface was negatively charged when the pH was 13. Moreover, ARG is an anionic dye, so it can be easily adsorbed onto the composite adsorbents pretreated with solutions in the pH range of 1–10, through simple electrostatic attractions. On the other hand, MB is a cationic dye, so apparently it can be effectively attracted by the alkali treated samples. Conversely, the removal efficiencies of ARG and MB were relatively low at pH of 13 and in the pH range of 1–10, respectively, because of the existence of electrostatic repulsion. In spite of that, these composites still can adsorb ARG or MB in these pH ranges, which may be attributed to the hydrogen bonding in the N–H groups contained in PPy molecules. Consequently, the composites would selectively adsorb ARG or MB by preprocessing the composites with acid or alkali solutions.

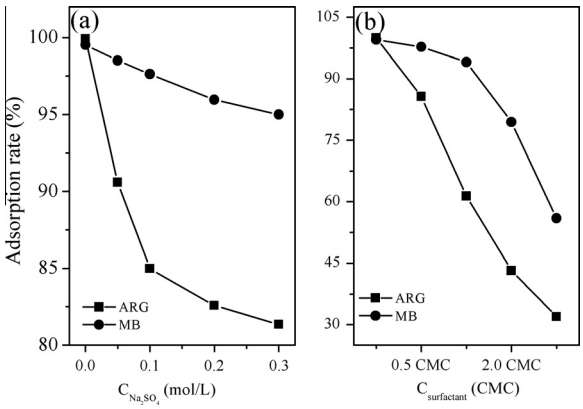

Fig. 6. Effects of ionic (a) and surfactant (b) concentrations on the adsorption capacity of 0.16 M-PPy/TiO_2.

3.2.2. Effect of ionic strength and surfactant on the adsorption capacity

As shown in Fig. 6a, the adsorption amounts of ARG and MB on 0.16 M-PPy/TiO_2 decrease with the increased Na_2SO_4 concentration. Zhang and Bai [10] and Lan et al. [26] indicated that the increase of ionic concentration would bring about the contraction of adsorbents, decrease the pore size of adsorbents, reduce the electrostatic attraction between the adsorbates and adsorbents, and also weaken the electrostatic repulsion between the adsorbates. The former three factors can decrease the adsorption capacity, while the last one can enhance the adsorption ability. Compromised among these four aspects, the adsorption capacity of 0.16 M-PPy/TiO_2 finally displayed a downward trend with the increase in salt concentration. Besides, it was also noted that the effect of ionic strength on ARG adsorption was larger than that on MB adsorption, because of the existence of the strong competitive adsorption between the introduced SO_4^{2-} groups and the anionic ARG molecules.

The effect of surfactant on the adsorption of ARG and MB is displayed in Fig. 6b. The adsorption amount of ARG or MB decreases with the rising SDBS or CTAB concentration, respectively. This can be explained from the following aspects: (a) surfactants can competitively adsorb with ARG or MB; (b) surfactants may occupy and reduce the active sites of adsorbents; and (c) ARG or MB may take part in the formation of micelles of surfactants, which enhanced the molecular size of ARG or MB. Additionally, it was also noted that the effect of surfactant on the adsorption of ARG was more obvious than that of MB. This may be related to the micelle sizes and shapes of SDBS and CTAB and the properties of ARG and MB.

3.2.3. Adsorption kinetics

Apart from possessing a high adsorption capacity, it is essential for an adsorbent to exhibit rapid adsorption kinetics in removing adsorbate from solution. Fig. 7 represents the influence of contact time on the adsorption of ARG and MB on the four composites. It was obvious that the adsorption of ARG or MB was rapid, and PPy/P25 needed a longer adsorption equilibrium time than the PPy/TiO_2 composites did.

The adsorption kinetics of ARG and MB are displayed in Fig. S2. From the plots, the related parameters are calculated and listed in Table 3. According to the values of the correlation coefficients, the adsorption behaviors of the four composites can be well described by the pseudo-second-order model (R^2 = 0.9976–1). Furthermore, the calculated values of Q_{eq} from the pseudo-second-order model approximately equal to the experimentally obtained values. This indicated that the adsorption kinetics of the four composites corresponded well with the pseudo-second-order model. Additionally, the initial adsorption rate, h_0 (mg/g/min) can be defined as:

$$h_0 = K_2 Q_{eq}^2 (T \rightarrow 0) \tag{10}$$

It was noted that the three PPy/TiO_2 composites possessed larger initial adsorption rate (h_0) than PPy/P25, especially the 0.16 M-PPy/TiO_2 composite, suggesting that the PPy/TiO_2 composites could reach adsorption equilibrium within a shorter period of time. Additionally, the initial adsorption rate of MB was larger than that of ARG, which suggests that MB can be adsorbed on the surface of the PPy/TiO_2 composites more easily. This may be due to the

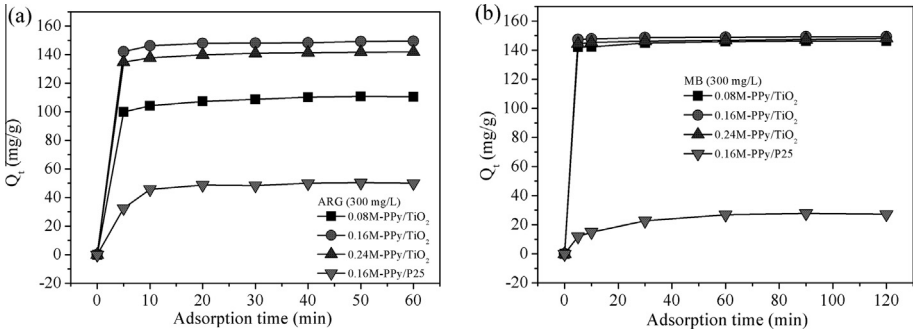

Fig. 7. Adsorption equilibrium curves of ARG (a) and MB (b) on the PPy/TiO_2 and PPy/P25 composites.

Table 3
Kinetic parameters of ARG and MB adsorption on the PPy/TiO_2 and PPy/P25 composites.

Dye	Adsorbent	First-order model			Second-order model			
		K_1	Q_{eq}	R^2	K_2	Q_{eq}	h_0	R_2
ARG	0.08 M-PPy/TiO_2	0.041	11.90	0.9172	0.012	111.98	150.47	0.9999
	0.16 M-PPy/TiO_2	0.045	6.85	0.9055	0.022	149.92	494.47	0.9999
	0.24 M-PPy/TiO_2	0.043	7.68	0.9633	0.019	142.65	142.65	0.9999
	PPy/P25	0.035	11.28	0.6838	0.0096	52.06	26.02	0.9988
MB	0.08 M-PPy/TiO_2	0.027	4.97	0.9570	0.026	146.63	559.01	1.000
	0.16 M-PPy/TiO_2	0.023	2.03	0.9322	0.054	149.48	1206.59	1.000
	0.24 M-PPy/TiO_2	0.019	3.83	0.9617	0.023	148.14	504.75	0.9999
	PPy/P25	0.019	14.46	0.7866	0.0042	29.55	3.67	0.9976

Table 4
Parameters of Langmuir and Freundlich adsorption isotherm models.

Dye	Adsorbents	Langmuir model				Freundlich model		
		Q_{max}	K_L	R^2	R_L	K_F	n	R^2
ARG	0.08 M-PPy/TiO_2	139.27	0.15	0.9843	0.016	63.30	0.15	0.9747
	0.16 M-PPy/TiO_2	218.82	0.20	0.9948	0.0083	146.59	0.069	0.9118
	0.24 M-PPy/TiO_2	187.62	0.28	0.9994	0.0059	116.04	0.092	0.8669
	PPy/P25	58.96	0.81	0.9997	0.0068	40.89	0.089	0.9662
MB	0.08 M-PPy/TiO_2	265.25	0.11	0.9873	0.015	97.59	0.20	0.9893
	0.16 M-PPy/TiO_2	323.62	0.071	0.9993	0.017	102.09	0.22	0.9832
	0.24 M-PPy/TiO_2	207.90	0.25	0.9979	0.0066	138.07	0.074	0.9955
	PPy/P25	48.66	1.01	0.9990	0.0081	22.03	0.28	0.6705

different molecular sizes of ARG and MB. The bigger ARG molecule hindered it from penetrating into the adsorbent mesoporous structure.

3.2.4. Adsorption isotherm

In order to describe the interaction between adsorbate and adsorbent, the adsorption isotherm was investigated. Fig. S3 shows the linear forms of Langmuir and Freundlich models. It was clearly exhibited that the degree of linearity of Langmuir adsorption isotherm model was better than that of Freundlich adsorption isotherm model. To be more specific, the experimental parameters of Freundlich and Langmuir isotherm models are listed in Table 4. It is obvious that the adsorption behaviors of the four composites for ARG and MB are appointed to the Langmuir isotherm, for its correlation coefficient R^2 is greater than that of Freundlich model. Besides, the dimensionless separation factor, R_L, which is an essential characteristic of the Langmuir model for reflecting the favorability of an adsorption process is used, expressed as:

$$R_L = \frac{1}{1 + K_L C_m} \tag{11}$$

where C_m is the maximum initial concentration of ARG or MB in solution. The R_L values were calculated and listed in Table 4. The values of R_L for the four composites were found to be in the range of 0–1, indicating that the adsorption processes were favorable.

Comparing the maximum adsorption amounts, the PPy/TiO_2 composites have better adsorption capacities than PPy/P25. This was related with the metal oxide properties to some extent. As indicated in the XRD results before, the PPy/TiO_2 composites were mainly amorphous state. Thus, the surface of TiO_2 in the PPy/TiO_2 composites possessed more defects than P25, and these defects would make TiO_2 coordinating with SO_4^{2-}, through which PPy was chemically connected with TiO_2 [27]. This can also be demonstrated by the FT-IR spectra of the self-prepared TiO_2 and P25 (as shown in Fig. S4). The three peaks located around 1200–900 cm^{-1} for TiO_2 prepared in different H_2SO_4 concentrations were assigned to the bidentate sulfate ions coordinated with metals such as Ti^{4+} [28]. The existence of the chemical interaction may give rise to more active sites, followed by improving the adsorption capacities of the three PPy/TiO_2 composites. Among all the adsorbents, the 0.16 M-PPy/TiO_2 composite possessed the largest Q_{max} of MB and ARG, indicating that the concentration of the used H_2SO_4 solution during the preparation process played a crucial role in the adsorption capacity. During the preparation process of TiO_2, low pH environment can enhance the rate of hydrolysis and defer the rate of condensation of TBOT, and also hinder the aggregation

Table 5
Comparison of the adsorption capacity of PPy/TiO_2 with other adsorbents for ARG and MB.

Dyes	Adsorbents	Q_{max} (mg/g)	Equilibrium time (h)	References
ARG	PPy/TiO_2	218.82	0.5	This work
	Coal fly ash	92.59	3	[30]
	Montmorillonite	171.53	1	[31]
MB	PPy/TiO_2	323.62	0.25	This work
	Bamboo-based activated carbon	454	48	[7]
	Activated carbon	270	>400	[8]

of the prepared TiO_2 [16,29]. This led to the prepared TiO_2 particles exhibiting different natures. On the other hand, the H_2SO_4 concentration can also impact the polymerization rate of pyrrole monomers. The polymerization rate of pyrrole monomers was comparatively slow in the lower H_2SO_4 concentration (0.08 mol/L), leading to a much denser and smaller pore structure of PPy. The higher concentration (0.24 mol/L) could enhance the polymerization rate, resulting in the obvious aggregation of PPy, and then reducing the effective sites. This can be confirmed by the SEM images (as shown in Fig. S5). In consequence, 0.16 mol/L of H_2SO_4 solution was appropriate. Hence, choosing the appropriate H_2SO_4 concentration and metal oxide were necessary.

Table 5 lists the adsorption capacities of several adsorbents for the removal of ARG and MB. It can be seen that the adsorption capacity of 0.16 M-PPy/TiO_2 is satisfied when compared with some other adsorbents already reported in literatures. Moreover, the equilibrium adsorption time of 0.16 M-PPy/TiO_2 in our experiments was less than that of other adsorbents. These results suggest that the PPy/TiO_2 adsorbent we prepared had more efficient adsorption capacity, and can be considered as a promising adsorbent for the removal of dye from wastewater. Based on the different maximum adsorption amount with different dyes, our results suggest that PPy/TiO_2 is more efficient in removing cationic dyes.

3.2.5. Thermodynamic analysis

From above results, 0.16 M-PPy/TiO_2 possessed the largest adsorption capacity. Therefore, it was chosen to study the thermodynamic property. The thermodynamic parameters such as changes in standard Gibbs free energy (ΔG°), entropy (ΔS°) and enthalpy (ΔH°) for the adsorption of ARG and MB by 0.16 M-PPy/TiO_2 were determined by the following equations:

$$\ln K_L = \frac{\Delta S^\circ}{R} + \frac{-\Delta H^\circ}{RT} \quad (12)$$

$$\Delta G^\circ = -RT \ln K_L \quad (13)$$

where R (kJ/mol/K) is the gas constant, and T (K) is the temperature. K_L (L/mg) is the constant of the Langmuir model. The related parameters were calculated and listed in Table 6. The positive value of ΔH° indicates that the process is endothermic in nature, while the positive value of ΔS° suggests that the disorder is increased at the solid-solution interface during the adsorption of dye. The decrease in ΔG° values with the increasing temperature determines that the adsorption process is spontaneous. Besides, the related parameters of the adsorption of ARG and MB were different, which may be attributed to the different properties of ARG and MB.

3.3. Regeneration experiments

According to the effect of the surface potential on the adsorption, the alkali or acid solutions can be considered as the desorption agents for ARG or MB adsorbed on 0.16 M-PPy/TiO_2, respectively, and the corresponding desorption efficiencies are listed in Table 7. Anhydrous ethanol has the lowest desorption efficiency, which may be due to lower wettability towards the composite in pure solvent [33]. The desorption efficiency of the pure acid or alkali solution is lower than that of the acid or alkali solution containing ethanol in the same concentration. This may be attributed to the similar consistency principle and electrostatic repulsion. Additionally, the desorption efficiency increased with the rising NaOH or HNO_3 concentration, probably because the surface of 0.16 M-PPy/TiO_2 would adsorb more OH^- and H^+ groups, which enhanced the electrostatic repulsion force between dye molecules and adsorbents. From Table 7, the optimal regeneration agents for MB and ARG were CH_3COOH (1.0 mol/L) and NaOH/ethanol solutions (volume ratio = 1:4, 0.01 mol/L), respectively. In comparison with the regeneration efficiency of activated carbon (as shown in Table 8), the results demonstrated that the PPy/TiO_2 adsorbent we prepared possessed a high desorption efficiency, and the regeneration method was available.

Afterwards, the desorbed adsorbents were treated with acid and alkali solutions as the activators, for ARG and MB, respectively. Then the regenerated adsorbents were utilized again to adsorb the same concentration of ARG and MB solutions to study its adsorption stability, as shown in Fig. 8. It can be seen that the removal efficiencies of ARG or MB by 0.16 M-PPy/TiO_2 were almost unchanged after regeneration for six times. This suggests that this composite possessed excellent adsorption capacity and stability.

3.4. Adsorption of dye effluent

Fig. 9 shows the decolorization efficiencies of ARG (pH = 4.5) and MB (pH = 9.5) in real effluents by 0.16 M-PPy/TiO_2. The results indicate that 0.16 M-PPy/TiO_2 had weaker adsorption capacity for ARG and MB effluents than for ARG and MB solutions, which may be ascribed to the complexity of the real effluent. In spite of that, the decolorization efficiencies of ARG and MB in real effluents

Table 6
Thermodynamic parameters of ARG and MB adsorption on 0.16 M-PPy/TiO_2.

Dye	Temperature (K)	K_L (L/mg)	ΔG° (kJ/mol)	ΔS° (J/mol/K)	ΔH° (kJ/mol)
ARG	288	0.12	−9.70	186.50	43.99
	298	0.20	−11.57		
	308	0.38	−13.43		
MB	288	0.045	−6.16	176.50	44.68
	298	0.071	−7.92		
	308	0.14	−9.69		

Table 7
Desorption efficiencies of ARG and MB by different desorption agents.

ARG		MB	
Desorption agent	DE (%)	Desorption agent	DE (%)
0.1 mol/L NaOH	90.59	0.1 mol/L HNO_3	53.82
0.01 mol/L NaOH	61.35	0.01 mol/L HNO_3	39.74
20% Ethanol + 0.01 mol/L NaOH	77.42	20% Ethanol + 0.01 mol/L HNO_3	68.16
40% Ethanol + 0.01 mol/L NaOH	87.50	40% Ethanol + 0.01 mol/L HNO_3	70.77
60% Ethanol + 0.01 mol/L NaOH	92.14	60% Ethanol + 0.01 mol/L HNO_3	73.19
80% Ethanol + 0.01 mol/L NaOH	97.39	80% Ethanol + 0.01 mol/L HNO_3	60.54
Anhydrous ethanol	6.15	Anhydrous ethanol	22.20
		1.0 mol/L CH_3COOH	85.21

Table 8
Comparison of desorption efficiencies of PPy/TiO_2 and other adsorbents.

Adsorbent	Adsorbate	Desorption method	DE (%)	Reference
PPy/TiO_2	Acid Red G	80% Ethanol + 0.01 M NaOH, 25 °C, 1 h	97.39	This work
	Methylene blue	1.0 mol/L CH_3COOH, 25 °C, 1 h	85.21	This work
Activated carbon	Peach red	60% Acetone, 25 °C, 100 h	58	[32]
	Mustard yellow	40% Isopropanol, 25 °C, 100 h	88	
	Methylene blue	0.1 mol/L NaOH, 25 °C, 48 h	75.1	[33]
	Methylene blue	Electrochemistry, 25 °C, 12 h	91.1	
	Congo red	Surfactant, 2500 mg/L, 30 °C	65	[34]
	Brilliant blue R	Wet oxidation, 150–250 °C, 3 h	91.2–98.7	[35]
	Phenol	Photocatalytic, 50 °C, 72 h	78.4	[36]
	p-Nitrophenol	Thermo, 300–850 °C, 3–5 h	60–70	[37]
	Phenol	Microwave, 1000 °C, 4 h	70–80	[38]

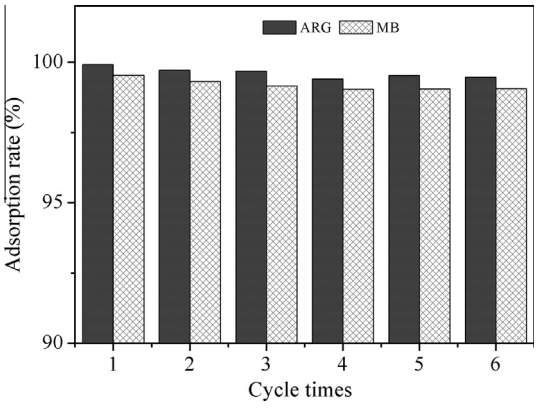

Fig. 8. Adsorption stabilities of 0.16 M-PPy/TiO_2 for 300 mg/L of ARG and MB in aqueous solutions.

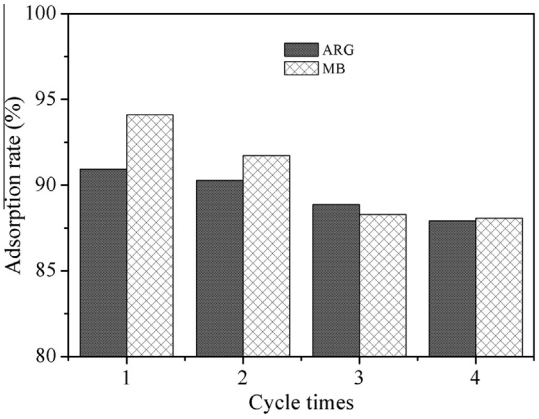

Fig. 9. Adsorption stabilities of 0.16 M-PPy/TiO_2 for 300 mg/L of ARG and MB in real effluents.

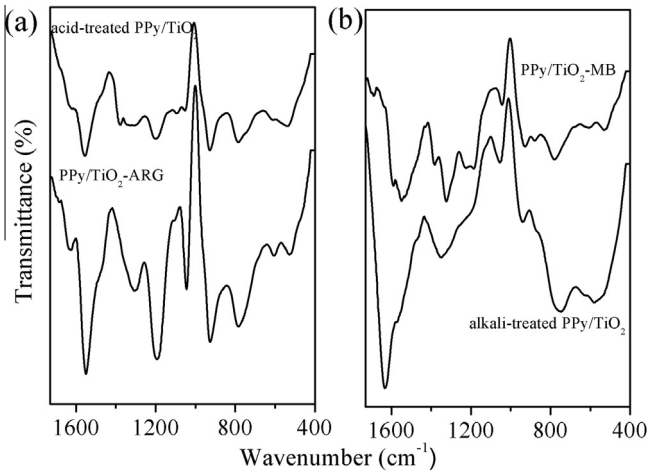

Fig. 10. FT-IR spectra of acid-treated 0.16 M-PPy/TiO_2 before and after adsorption ARG (a) and alkali-treated 0.16 M-PPy/TiO_2 before and after adsorption MB (b).

were still higher than 87% after adsorption–desorption for four times. These results indicate that 0.16 M-PPy/TiO_2 also possessed efficient adsorption capacity for ARG and MB in real effluents.

3.5. Adsorption mechanism

Dye molecule adsorption on the adsorbents may proceed through physical, chemical or combination of both at the interfaces. FT-IR analysis was conducted to examine the possible existence of the chemical interaction in the adsorption process, as shown in Fig. 10. Liang et al. [39] proposed that the relative intensities of the bands at 1550 and 1470 cm^{-1} are particularly sensitive to the extent of charge delocalization. Zhang et al. [11] compared the ratio changes in the intensities of bands at 1550 and 1470 cm^{-1} of PPy before and after the protein adsorption, and indicated that the chemical interaction directly existed between PPy

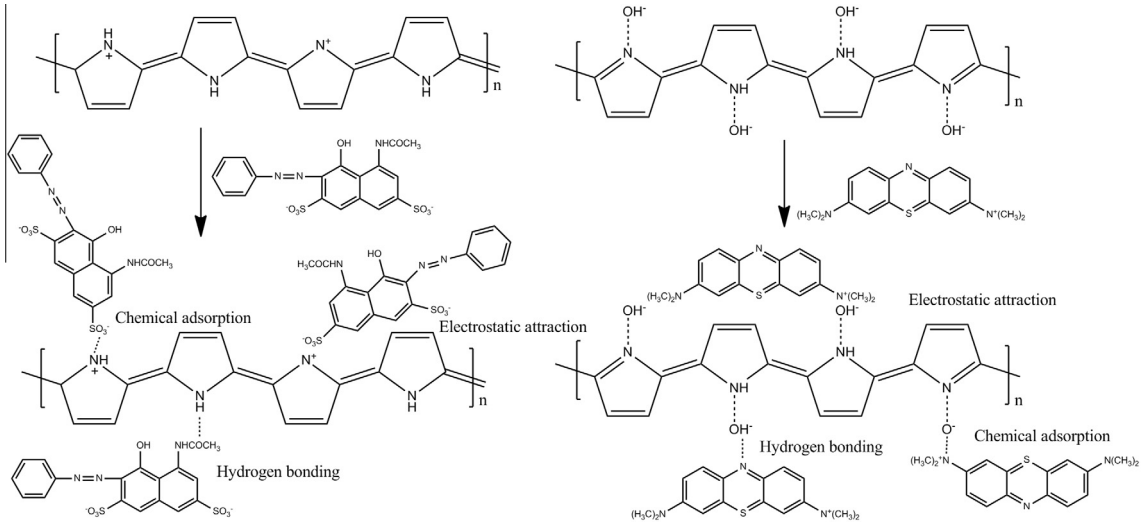

Scheme 1. The plausible mechanism for the removal of ARG and MB from aqueous solution.

backbone and proteins. Hence, the ratio changes in the intensities of bands at 1550 and 1470 cm^{-1} in Fig. 10 provided the evidence that ARG or MB molecules was chemically adsorbed on the surface of PPy/TiO_2. Besides, the peak at 1630 cm^{-1} in the spectrum of the alkali-treated PPy/TiO_2 composite is attributed to the hydroxyl groups disappeared after MB adsorption, which also suggests that MB was chemically adsorbed on the surface of PPy/TiO_2. Additionally, according to the previous analyses, adsorption of ARG or MB on PPy/TiO_2 also can utilize the electrostatic interaction and hydrogen bonding, and the electrostatic interaction playing the major role. The plausible mechanism for the removal of ARG and MB from aqueous solution was shown in Scheme 1 [10,11,40].

4. Conclusions

In this article, the adsorption and regeneration capacities of the PPy/TiO_2 and PPy/P25 composites prepared in different concentrations of H_2SO_4 were studied. The results revealed that the H_2SO_4 concentration and the property of metal oxide (self-prepared TiO_2 or commercial P25) obviously affected the nature and adsorption abilities of the prepared composites. XRD analyses suggested that the PPy/TiO_2 and PPy/P25 composites had different crystalline structures. FT-IR results suggested that they possessed different polymerization and doping levels. The results from TGA indicated that the PPy/TiO_2 composites contained higher content of PPy than PPy/P25 did. The adsorption results showed that the acid-treated adsorbents would prefer to adsorb ARG, while the alkali-treated adsorbents tended to adsorb MB. The adsorption capacities of the composites decreased with the increasing salt and surfactant concentrations. ARG and MB adsorption was rapid and it could reach the equilibrium within 30 min. The adsorption behaviors of ARG and MB on the composites were described by the pseudo-second-order and Langmuir isotherm models. The adsorption capacities, in the descending order of the maximum adsorption amount (Q_{max}), were 0.16 M-PPy/TiO_2, 0.24 M-PPy/TiO_2, 0.08 M-PPy/TiO_2 and PPy/P25. Thermodynamic parameters confirmed the spontaneous and endothermic nature of the adsorption process. Desorption experiments revealed that the NaOH ethanol (0.01 mol/L) and CH_3COOH (1.0 mol/L) solutions can be chosen as desorption agents for the composites adsorbed ARG and MB, respectively. The 0.16 M-PPy/TiO_2 composite still exhibited efficient adsorption capacities for ARG and MB after adsorption–desorption for six cycles. In addition, 0.16 M-PPy/TiO_2 still possessed outstanding adsorption capacity for ARG and MB in real effluents after regeneration for four times with the adsorption efficiency larger than 87%. Electrostatic interaction, hydrogen bonding and specific chemical interaction may play the role in ARG and MB adsorption performance. Finally, the influence of the properties of metal oxide on the adsorption capacity of the composite adsorbents will be further investigated.

Acknowledgements

The authors gratefully acknowledge the financial supports from the Fundamental Research Funds for the Central Universities of China, the Specialized Research Fund for the Doctoral Program of Higher Education of China (20090201110005), and the Science and Technology Project of Wenzhou, PR China (H2010004).

Appendix A. Supplementary material

Supplementary data associated with this article can be found, in the online version, at http://dx.doi.org/10.1016/j.cej.2013.03.011.

References

[1] M. Janus, E. Kusiak, J. Choina, J. Ziebro, A.W. Morawski, Enhanced adsorption of two azo dyes produced by carbon modification of TiO_2, Desalination 249 (2009) 359–363.
[2] S. Asuha, X.G. Zhou, S. Zhao, Adsorption of methyl orange and Cr(VI) on mesoporous TiO_2 prepared by hydrothermal method, J. Hazard. Mater. 181 (2010) 204–210.
[3] K. Bourikas, M. Stylidi, D.I. Kondarides, X.E. Verykios, Adsorption of Acid Orange 7 on the surface of titanium dioxide, Langmuir 21 (2005) 9222–9230.
[4] M. Janus, J. Choina, A.W. Morawski, Azo dyes decomposition on new nitrogen-modified anatase TiO_2 with high adsorptivity, J. Hazard. Mater. 166 (2009) 1–5.
[5] V. Belessi, G. Romanosa, N. Boukosa, D. Lambropouloud, C. Trapalis, Removal of Reactive Red 195 from aqueous solutions by adsorption on the surface of TiO_2 nanoparticles, J. Hazard. Mater. 170 (2009) 836–844.
[6] X.L. Tan, M. Fang, J.X. Li, Y. Lu, X.K. Wang, Adsorption of Eu(III) onto TiO_2: effect of pH, concentration, ionic strength and soil fulvic acid, J. Hazard. Mater. 168 (2009) 458–465.
[7] B.H. Hameed, A.L. Ahmad, A.T.M. Din, Adsorption of methylene blue onto bamboo-based activated carbon: kinetics and equilibrium studies, J. Hazard. Mater. 141 (2007) 819–825.
[8] B.H. Hameed, A.L. Ahmad, K.N.A. Latiff, Adsorption of basic dye (Methylene blue) onto activated carbon prepared from rattan sawdust, Dyes Pigm. 75 (2007) 143–149.
[9] Q.L. Cheng, Y. He, V. Pavlinek, C.Z. Li, P. Saha, Surfactant-assisted polypyrrole/titanate composite nanofibers: morphology, structure and electrical properties, Synth. Met. 158 (2008) 953–957.
[10] X. Zhang, R.B. Bai, Adsorption behavior of humic acid onto polypyrrole-coated nylon 6, 6 granules, J. Mater. Chem. 12 (2002) 2733–2739.

[11] X. Zhang, R.B. Bai, Y.W. Tong, Selective adsorption behaviors of proteins on polypyrrole-based adsorbents, Sep. Purif. Technol. 52 (2006) 161–169.
[12] S.K. Bajpai, V.K. Rohit, M. Namdeo, Removal of phosphate anions from aqueous solutions using polypyrrole-coated sawdust as a novel sorbent, J. Appl. Polym. Sci. 111 (2009) 3081–3088.
[13] M. Karthikeyan, K.K. Satheeshkumar, K.P. Elango, Removal of fluoride ions from aqueous solution by conducting polypyrrole, J. Hazard. Mater. 167 (2009) 300–305.
[14] Q.B. Pei, R.Y. Qian, Protonation and deprotonation of polypyrrole chain in aqueous solutions, Synth. Met. 45 (1991) 35–48.
[15] X. Zhang, R.B. Bai, Surface electric properties of polypyrrole in aqueous solutions, Langmuir 19 (2003) 10703–10709.
[16] K.A. Dunphy-Guzman, M.P. Finnegan, J.F. Banfield, Influence of surface potential on aggregation and transport of titania nanoparticles, Environ. Sci. Technol. 40 (2006) 7688–7693.
[17] Z.L. Tang, J.Y. Zhang, Z. Cheng, Z.T. Zhang, Synthesis of nanosized rutile TiO_2 powder at low temperature, Mater. Chem. Phys. 77 (2002) 314–317.
[18] M.A. Ulibarri, I. Pavlovic, C. Barriga, M.C. Hermosín, J. Corneio, Adsorption of anionic species on hydrotalcite-like compounds: effect of interlayer anion and crystallinity, Appl. Clay Sci. 18 (2001) 17–27.
[19] X.F. Xie, L. Gao, Effect of crystal structure on adsorption behaviors of nanosized TiO_2 for heavy-metal cations, Curr. Appl. Phys. 9 (2009) S185–S188.
[20] D.S. Wang, Y.H. Wang, X.Y. Li, Q.Z. Luo, J. An, J.X. Yue, Sunlight photocatalytic activity of polypyrrole–TiO_2 nanocomposites prepared by 'in situ' method, Catal. Commun. 9 (2008) 1162–1166.
[21] N.V. Blinova, J. Stejskal, M. Trchová, J. Prokeš, M. Omastová, Polyaniline and polypyrrole: a comparative study of the preparation, Eur. Polym. J. 43 (2007) 2331–2341.
[22] X.M. Feng, Z.Z. Sun, W.H. Hou, J.J. Zhu, Synthesis of functional polypyrrole/prussian blue and polypyrrole/Ag composite microtubes by using a reactive template, Nanotechnology 18 (2007) 195603.
[23] X.Y. Li, D.S. Wang, G.X. Cheng, Q.Z. Luo, J. An, Y.H. Wang, Preparation of polyaniline-modified TiO_2 nanoparticles and their photocatalytic activity under visible light illumination, Appl. Catal. B 81 (2008) 267–273.
[24] C. Lai, G.R. Li, Y.Y. Dou, X.P. Gao, Mesoporous polyaniline or polypyrrole/anatase TiO_2 nanocomposites as anodematerials for lithium-ion batteries, Electrochim. Acta 55 (2010) 4567–4572.
[25] M. Omastová, M. Trchová, J. Kovářová, J. Stejskal, Synthesis and structural study of polypyrrole prepared in the presence of surfactants, Synth. Met. 138 (2003) 447–455.
[26] Q.D. Lan, A.S. Bassi, J.X. Zhu, A modified Langmuir model for the prediction of the effects of ionic strength on the equilibrium characteristics of protein adsorption onto ion exchange/affinity sorbents, Chem. Eng. J. 81 (2001) 179–186.
[27] Q.L. Zhang, L.C. Du, Y.X. Weng, L. Wang, H.Y. Chen, J.Q. Li, Particle-size-dependent distribution of carboxylate adsorption sites on TiO_2 nanoparticle surfaces: insights into the surface modification of nanostructured TiO_2 electrodes, J. Phys. Chem. B 108 (2004) 15077–15083.
[28] J.R. Sohn, S.H. Lee, P.W. Cheon, H.W. Kim, Acidic properties and catalytic activity of titanium sulfate supported on TiO_2, Bull. Korean Chem. Soc. 25 (2004) 657–664.
[29] S. Termnak, W. Triampo, D. Triampo, Effect of acid during synthesis on the agglomerated strength of TiO_2 nanoparticles, J. Ceram. Process. Res. 10 (2009) 491–496.
[30] T.C. Hsu, Adsorption of an acid dye onto coal fly ash, Fuel 87 (2008) 3040–3045.
[31] D.S. Tong, C.H. Zhou, Y. Lan, H.Y. Yu, G.F. Zhang, W.H. Yu, Adsorption of Acid Red G on octadecyl Trimethylammonium montmorillonite, Appl. Clay Sci. 50 (2010) 427–431.
[32] P.J. Lu, H.C. Lin, W.T. Yu, J.M. Chern, Chemical regeneration of activated carbon used for dye adsorption, J. Taiwan Inst. Chem. Eng. 42 (2011) 305–311.
[33] C.H. Weng, M.C. Hsu, Regeneration of granular activated carbon by an electrochemical process, Sep. Purif. Technol. 64 (2008) 227–236.
[34] M.K. Purkait, A. Maiti, S. DasGupta, S. De, Removal of congo red using activated carbon and its regeneration, J. Hazard. Mater. 145 (2007) 287–295.
[35] R.V. Shenda, V.V. Mahajani, Wet oxidative regeneration of activated carbon loaded with reactive dye, Waste Manage. 22 (2002) 73–83.
[36] S.X. Liu, C.L. Sun, S.R. Zhang, Photocatalytic regeneration of exhausted activated carbon saturated with phenol, Bull. Environ. Contam. Toxicol. 73 (2004) 1017–1024.
[37] E. Sabio, E. González, J.F. González, C.M. González-García, A. Ramiro, J. Gañan, Thermal regeneration of activated carbon saturated with p-nitrophenol, Carbon 42 (2004) 2285–2293.
[38] X.T. Liu, X. Qian, L.L. Bo, S. Chen, Y.Z. Zhao, Simultaneous pentachlorophenol decomposition and granular activated carbon regeneration assisted by microwave irradiation, Carbon 42 (2004) 415–422.
[39] W. Liang, J. Lei, C.R. Martin, Effect of synthesis temperature on the structure, doping level and charge-transport properties of polypyrrole, Synth. Met. 52 (1992) 227.
[40] J. Wang, B. Deng, H. Chen, X.R. Wang, J.Z. Zheng, Removal of aqueous Hg(II) by polyaniline: sorption characteristics and mechanisms, Environ. Sci. Technol. 43 (2009) 5223–5228.